Ultramicroscopy 201 (2019) 68–76

Contents lists available at ScienceDirect

Ultramicroscopy

journal homepage: www.elsevier.com/locate/ultramic

Geometry determination and refinement in the rotation electron diffraction technique

Andreas Delimitis[a,*], Vidar Hansen[a], Jon Gjønnes[b]

[a] Department of Mechanical and Structural Engineering and Materials Science, University of Stavanger, N-4036, Stavanger, Norway
[b] Department of Physics, University of Oslo, Gaustadalleen 21, N-0371, Oslo, Norway

ARTICLE INFO

Keywords:
Rotation electron diffraction
RED
Dynamical diffraction
Structure determination
Kikuchi lines
Thermoelectric materials

ABSTRACT

The necessary parameters (rotation axis, incident electron beam direction and beam tilt path) in order to describe the diffraction geometry in the Rotation Electron Diffraction (RED) method during data collection are determined and refined. These parameters are prerequisites for the subsequent calculations of excitation errors, s_g, for zero (ZOLZ) or higher order Laue zones (HOLZ) reflections. Comparison with simulated results, for a CoP_3 thermoelectric crystal, shows excellent agreement between the two approaches -calculated and simulated. In addition to their determination, a thorough refinement methodology for the incident electron beam direction and beam tilt path has been applied, too, based on Kikuchi lines of HOLZ reflections. Incorporation of the refined excitation error values can be considered both in theoretical calculations for diffracted beam intensities, based on the Bloch wave method, as well as in deducing integrated intensities from experimental rocking curves. The methodology described in this study is quite indispensable, as it forms an essential step for performing dynamical calculations in RED, enabling thus enhanced accuracy in structural parameter clarification. The latter is especially important in the case of thermal factors refinement for e.g. thermoelectrics, which are imperative for material properties' evaluation.

1. Introduction

There has been an increasing interest in the use of electron diffraction based methods for structure determination and refinement in recent years. Among the methods developed, Precession Electron Diffraction (PED) [1] has been a real breakthrough, followed by Automated Diffraction Tomography (ADT) [2], which has been also combined with PED [3] and, more recently, Rotation Electron Diffraction (RED) [4]. This is merely due to their capability to obtain single crystal data from nanoscale materials, which can in principle, be more beneficial compared to results from powder X-ray (XRD) or neutron diffraction. The competence of these methods is based, among others, on the elimination efforts of dynamical interactions between the diffracted electron beams [1,3,4]; the latter has long been a limiting factor for accuracy enhancement in structure determination by electron diffraction.

Among these techniques, the applicability of the Rotation Electron Diffraction method for detailed structure analysis has been already broadly demonstrated [4-6]. In aid of the user, RED bears a resemblance with the methods widely used in single crystal X-ray diffractometers [7]. The method has been so far utilized for a wide range of materials, such as zeolites [8,9], supercapacitor chalcogenide nanowires [10], metal organic frameworks [11], porous multiphase powders [12], quasicrystals [13], etc. In recent years, a strong focus of RED applications in solving the structure of beam-sensitive materials, such as pharmaceuticals [14] has been arisen. This is predominately due to recent developments of the RED technique, such as continuous RED (cRED) [15], either in manual or automated data acquisition modes [16]; the latter has been aided much by the use of advanced electron imaging detectors [17]. In general, RED, along with Automated Diffraction Tomography (ADT) [2] additionally offers the acquisition of three dimensional (3D) electron diffraction patterns, facilitating thus structural studies from first principles (*ab initio*) calculations. RED has been predominately developed to collect 3D data in a large sector of the reciprocal space for crystal structure determination [4], in an analogous fashion as in single crystal XRD. Usually, PED collects data for integrated intensities measurements from zone axes orientations [1]. On the other hand, both ADT and RED methods often employ electron diffraction data collection in off zone axes orientations during experimental acquisition in the microscope, in order to extract more kinematical intensities than those achieved by electron diffraction patterns close to major zone axes orientations and at the Selected Area

* Corresponding author.
E-mail address: andreas.delimitis@uis.no (A. Delimitis).

https://doi.org/10.1016/j.ultramic.2019.02.011
Received 12 October 2018; Received in revised form 7 February 2019; Accepted 18 February 2019
Available online 19 February 2019

Diffraction (SAD) mode. However, certain dynamical effects are still present and, therefore, care must be taken to account for these remaining dynamical contributions, which significantly limit accuracy and result in poor reliability factor (R) values [18] in structure determination. The importance of method refinement is further illustrated when it comes to structure specific properties, such as accurate determination of thermal (i.e. Debye-Waller) factors of thermoelectric materials [19]. In such materials, control of their thermal conductivity is crucial for enhanced performance [20], consequently precise Debye-Waller factors calculations by electron diffraction methods is highly desirable.

Sinkler and Marks [21] pointed out the necessity of two or many beam dynamical intensity calculations in PED for precise structure determination. Up to then, either the two-beam approach, or kinematical ones were used [22] to calculate structure data from PED intensities in a comparative fashion. The same group, in a collaboration with Palatinus et al. [22] proceeded further, incorporating the Bloch wave formalism for intensities calculation and structure determination. In there, refinement of structures is accomplished by a series of non-oriented electron diffraction patterns obtained by Electron Diffraction Tomography (EDT), either PED or RED and fully dynamical approach (Bloch waves) to calculate intensities of the diffracted beams. In [21] it was clarified that, in every case diffraction intensities are averaged over the various off-axis orientations, there is a reduced sensitivity of them to structure factor phases, merely due to the inclination of the incident beam direction. Due to this, experimental data could directly provide structure factor moduli in both kinematical and two beam approaches. The authors have demonstrated [22] that, among the three approaches (kinematical, two- or many-beam one), it is the latter (many beam dynamical) that offers superiority in structure data refinement. Still, additional requirements in Bloch wave formalism, such as sample thickness or orientation accuracy, impose certain drawbacks in structure solution. It is merely this reason that researchers have also relied to the easier, more effortless kinematical strategies.

In addition, a number of inaccuracies may arise when collecting data, such as precise determination of the beam tilt angle in RED, imprecisions of the goniometer tilt movement, sample drifting or specimen electron beam sensitivity, etc. Consequently, several groups have developed various and sophisticated data collection strategies; for instance, cRED method by Zou's group, alone or combined with serial electron diffraction crystallography (SerialED) [16], in order to efficiently overcome those issues.

In previous works, the importance of geometrical factors associated with electron diffraction methods for structure determination has been already pointed out. Several groups outlined the necessity for accurate definition and corrections of the geometry in PED [23-26] or ADT [3], as an initial and definite step towards diffracted intensity corrections and structure factor acquisition. One significant advantage of RED is that its diffraction geometry is analogous with that of PED -in the broad sense that both methods initially involve deflection of the incident electron beam off the optical axis [5] in the microscope- and thus data analysis can be facilitated given some similarities in geometry between the two methods. Nevertheless, the analytical expressions derived for the determination of diffraction geometry in PED cannot be directly applied in RED as is and without considering the particularity of the latter method compared to the former. Palatinus and co-workers have previously dealt with geometry parameters for EDT (both ADT combined with PED, as well as RED) methods. However, although the similarities between PED and RED, especially in the general equations for excitation errors [26], analytical expressions are not exactly the same between them and therefore, such formulas need be derived for RED. In previous works [4,5,19] the rotation axis in a goniometer or beam tilting experiment was defined, using a variety of methods, however a robust description of the diffraction geometry in RED has yet to be established.

In this study, a definite step for incorporating dynamical interactions of the diffracted beams in RED for the precise determination of structural parameters is presented. This is achieved by a more exact description and refinement of the diffraction geometry, which is essential for integrated intensity measurements and dynamical structure factor calculations. As a continuation of rotation axis determination [19], precise calculations and refinement of the incident electron beam direction and beam tilt path will be herein described, by a combination of pattern analysis and simulation of Kikuchi lines from higher order Laue zone (HOLZ) reflections. HOLZ reflections are rather advantageous compared to zero order Laue zone ones (ZOLZ), as they bear a satisfactory 'kinematical' concept. Their Kikuchi lines can be effectively used for refinement, as they are quite sensitive to tilting, thus enabling calculations of crystal orientation with high precision. Expressions for calculating the excitation errors, $s_{\mathbf{g}}$, for ZOLZ and HOLZ reflections as a function of experimental tilt angle β of the incident beam will be also illustrated; such expressions can equally hold for sample/goniometer tilt experiments, too. These steps are rather essential, especially when comparing the experimental intensity measurements results with the theoretical ones -the latter derived by the Bloch wave method- and can ultimately lead to refinement of materials structure parameters. Crystallographic analyses of thermoelectric materials are currently among our major research interests [18,19] and precise determination of their structure, as far as thermal parameters (i.e. Debye-Waller factors) refinement is ultimately imperative. Therefore, results of this refinement strategy in the study of thermoelectrics will be presented and evaluated.

2. Material and methods

The sample under study was a CoP_3 binary skutterudite [19], grown by a flux technique in crystalline form. Binary skutterudites, have the general formula MX_3, where M is a transition metal and X a pnictogen atom. CoP_3 has a body centred cubic (bcc) structure (space group $Im\bar{3}$, #204), with the X atoms surrounding M atoms in octahedral coordination [27].

Samples suitable for TEM observations were prepared by mixing the material –in powder form- with high purity ethanol using an agate pestle and mortar. A drop of the solution was deposited onto a holey C film supported on a 300 mesh Cu grid and left to dry under ambient conditions. A JEOL JEM 2100 electron microscope, at Stockholm University, with an acceleration voltage of 200 kV was used. The RED experiments were collected in the SAD mode, using a combination of goniometer and beam tilts and at a random initial crystal orientation [19]. It has to be noted here that, any tilting angles values in parentheses at the calculations section illustrate the difference between the angle of each corresponding pattern and any experimentally encountered zone axis one, whereas numbers outside parentheses denote net experimental tilting angle values. SAD patterns were recorder in a bottom mounted Gatan SC1000 Orius CCD camera. Scripts developed in Gatan's Digital Micrograph software suite were used both for control of the TEM and camera and collection of experimental SAD patterns.

Calculations of RED diffraction geometry elements and their refinement was made feasible by self-developed packages in Python programming language, v3.2, using Python's IDLE Integrated Development Environment. Simulated SAD patterns, as well as the 'theoretical' values of the excitation errors were deduced by the JEMS software [28], version 4 (v4) for Windows platforms.

3. Theory

3.1. Determination and refinement of rotation axis $\boldsymbol{Y}$

One of the first attempts to clarify the geometry in the RED method has been the determination and refinement of the rotation axis, $\boldsymbol{Y}$, during an experiment. This was described in previous works [5,19], where several alternative ways to determine $\boldsymbol{Y}$ were proposed. Among

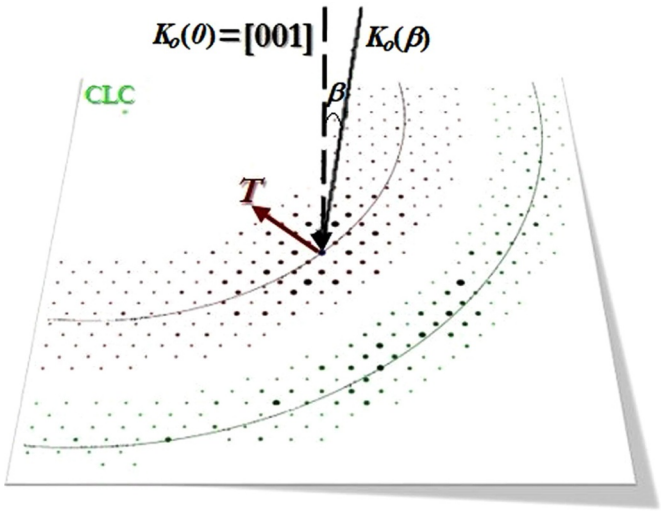

Fig. 1. The change of the incident electron beam direction as a function of tilting angle β during a RED goniometer tilt experiment. $\boldsymbol{K_o(0)}$ was along the $\boldsymbol{Z}$ = [001] zone axis. CoP_3 reflections from the ZOLZ (red) and FOLZ (green) and their corresponding Laue circles are also illustrated. (For interpretation of the references to colour in this figure legend, the reader is referred to the web version of this article.)

them, attention is drawn here to the calculation of $\boldsymbol{Y}$ using two non-integer zone axis patterns [19], during a RED goniometer tilt experiment. Choosing this way defines $\boldsymbol{Y}$ with significantly higher accuracy compared to the other ways described in [19]; additionally, it serves as a method for refining the rotation axis, too.

3.2. Theoretical aspects of diffraction geometry

A simplified, general case for an arbitrary diffraction pattern near a zone axis in a tilting TEM experiment is illustrated in Fig. 1. In there, the incident (direct) beam $\boldsymbol{K_o(0)}$ has been chosen to be parallel to the zone axis $\boldsymbol{Z}$ = [uvw]. It has to be stated here that this choice was merely due to reference purposes for our following calculations, i.e. *not* by the beginning of experimental data acquisition. The projection of the centre of the Ewald sphere at the ZOLZ plane denotes the centre of the corresponding Laue circle, which is illustrated as CLC in the figure. Since this ZOLZ plane will form the basis of our calculations, its importance has to be explicitly demonstrated and it will be further proved in the following.

In order to precisely describe and, thus, greatly facilitate our analysis, a 'reference plane' is defined and every vector is designated accordingly. The ZOLZ zone axis pattern was chosen as the 'reference plane' and three unit vectors $\boldsymbol{u_1}$, $\boldsymbol{u_2}$, $\boldsymbol{u_3}$ were utilised; the latter two define this plane and $\boldsymbol{u_1}$ is perpendicular to it. In general, the three reciprocal lattice vectors closer to the origin are selected as the $\boldsymbol{u_1}$, $\boldsymbol{u_2}$, $\boldsymbol{u_3}$ vectors. Consequently, any vector in reciprocal space can be analysed into components of these three unit vectors; for instance, a reciprocal lattice vector $\boldsymbol{g_i}$ takes the form:

$$\boldsymbol{g_i} = g_{i1}\boldsymbol{u}_1 + g_{i2}\boldsymbol{u}_2 + g_{i3}\boldsymbol{u}_3 \tag{1}$$

The vectors $\boldsymbol{u_2}$ and $\boldsymbol{u_3}$ must not be parallel; however, they need not be perpendicular to each other. The $\boldsymbol{u_1}$ vector is perpendicular to the plane defined by $\boldsymbol{u_2}$ and $\boldsymbol{u_3}$. This methodology has been incorporated in all equations derived in the manuscript and a characteristic example of this analysis is given in Appendix A.

In the RED method, it is highly essential to define a universal relationship that describes the change of the incident beam direction as a function of the tilting angle beta (β), i.e. $\boldsymbol{K_o(\beta)}$. This is merely envisaged by introducing an additional new vector $\boldsymbol{T}$, as depicted in Fig. 1 [3]. $\boldsymbol{T}$ is the projected electron beam trace or, in other words, the projected beam tilt path in ZOLZ during the RED experiment. $\boldsymbol{K_o(\beta)}$ is then calculated by:

$$\boldsymbol{K_o}(\beta) = \boldsymbol{K_o}(0) + n\beta\,\boldsymbol{T} \tag{2}$$

where n is a normalization factor, in order to account for the different values of the magnitudes of the $\boldsymbol{K_o}$ and $\boldsymbol{T}$ vectors. In more detail, all terms in Eq. (2) have to be normalized by the magnitude of the $\boldsymbol{K_o(0)}$ vector, which is $|\boldsymbol{K_o(0)}| = 1/\lambda$, with λ being the wavelength of the high energy electron beam in TEM. The tilting angle β in this equation refers to beam or goniometer tilts alike and is expressed in radians (rad). An example of the $\boldsymbol{K_o(\beta)}$ determination is provided in Appendix B, as a substantial step prior to excitation errors calculation.

The beam tilt path is also related to the rotation axis $\boldsymbol{Y}$ [19] by the following formula:

$$\boldsymbol{T} = \boldsymbol{Y} \times \boldsymbol{Z} \tag{3}$$

with $\boldsymbol{Z}$ being the initial zone axis, for which the tilt angle is considered $\beta = 0$. Eq. (3) is a rather simple and useful formula, which can be applied to commonly encountered experimental cases.

3.3. Expressions for excitation errors s_g for ZOLZ and HOLZ reflections

Having defined the aforementioned quantities ($\boldsymbol{T}$ and $\boldsymbol{K_o(\beta)}$), a general expression for the excitation errors s_g, can be derived, as well. Expressions for excitation errors in PED have been already deduced [21,25,26]. The starting point is the well-known equation for s_g (see Fig. 2):

$$\boldsymbol{K_o} + \boldsymbol{g} = \boldsymbol{K_g} = \boldsymbol{K_o} - s_g \tag{4}$$

$$2ks_g = -2\boldsymbol{K_o}\cdot\boldsymbol{g} - \boldsymbol{g}^2 \tag{5}$$

In these formulas, $\boldsymbol{K_o}$ and $\boldsymbol{K_g}$ are the incident and diffracted -from a (hkl) plane- beam vectors. Eq. (5) is slightly modified, to account for beam or goniometer tilting experiments in RED:

$$2ks_g = -2\boldsymbol{K_o}(\beta)\cdot\boldsymbol{g} - \boldsymbol{g}^2 \tag{6}$$

where $k = |\boldsymbol{K_o(0)}| = 1/\lambda$ and $\boldsymbol{g}$ can be any diffraction vector, either from ZOLZ or HOLZ. By substituting Eq. (2), two analytical expressions are derived:

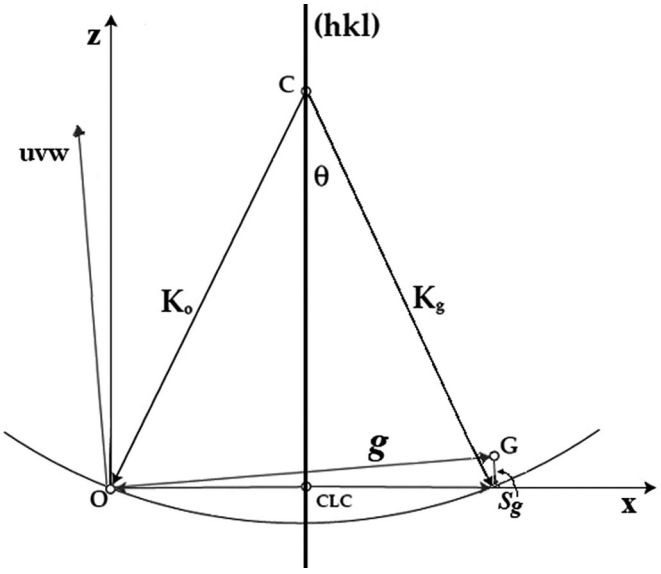

Fig. 2. Schematic definition of excitation errors s_g in electron diffraction [28]. θ is the diffraction angle (not exactly in Bragg conditions) and O and G define the direct and one diffracted reciprocal lattice points. The centre of the Ewald sphere and its projection in the ZOLZ plane (the Laue circle centre) are denoted by C and CLC, respectively.

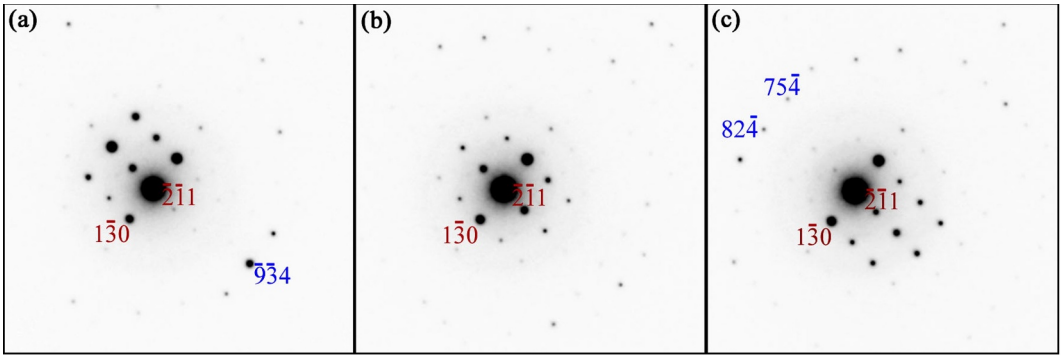

Fig. 3. Three typical experimental SAD patterns (contrast inverted), acquired from the series of the RED beam tilting experiment. Characteristic ZOLZ and SOLZ reflections are denoted by red and blue indices in the patterns, respectively. (For interpretation of the references to colour in this figure legend, the reader is referred to the web version of this article.)

Table 1
Calculation results of $\boldsymbol{K_o(\beta)}$ as a function of the tilting angle β in relation to the one of the main zone axis, [0 0 1] or [$\bar{3}$ $\bar{1}$ $\bar{7}$] in each case.

[uvw] = [0 0 1] $\boldsymbol{Y}$ ~ [$\bar{1}$ $\bar{1}$ 0]			[uvw] = [$\bar{3}$ $\bar{1}$ $\bar{7}$] $\boldsymbol{Y}$ ~ [1 $\bar{3}$ 0]		
	β (°)	$\boldsymbol{K_o(\beta)}$		β (°)	$\boldsymbol{K_o(\beta)}$
1	−0.10	[0.001 $\overline{0.001}$ $\bar{1}$]	1	−0.05	[3 1 6.987]
2	−0.35	[0.003 $\overline{0.003}$ $\bar{1}$]	2	−0.50	[2.999 1 6.876]
3	−0.80	[0.008 $\overline{0.008}$ $\bar{1}$]	3	−1.35	[2.999 1 6.675]
4	−1.25	[0.001 $\overline{0.001}$ $\bar{1}$]	4	−2.40	[2.999 1 6.439]
5	0	[0 0 $\bar{1}$]	5	0	[3 1 7]
6	0.25	[$\overline{0.002}$ 0.002 $\bar{1}$]	6	0.60	[3 1 7.153]
7	0.45	[$\overline{0.004}$ 0.004 $\bar{1}$]	7	1.85	[2.999 1 7.491]
8	0.90	[$\overline{0.008}$ 0.008 $\bar{1}$]	8	2.10	[3 1 7.561]
9	1.70	[$\overline{0.016}$ 0.016 $\bar{1}$]	9	3.50	[2.999 1 7.979]
10	4.25	[$\overline{0.040}$ 0.040 $\bar{1}$]	10	4.15	[2.999 1 8.186]

$$2\mathrm{ks}_g = -2n\beta \boldsymbol{T}\cdot\boldsymbol{g} - \boldsymbol{g}^2 \quad (7)$$

$$2\mathrm{ks}_g = -2n\beta \boldsymbol{T}\cdot\boldsymbol{g_t} - 2\boldsymbol{K_o}(0)\cdot\boldsymbol{g_n} - \boldsymbol{g}^2 \quad (8)$$

Eq. (7) is valid for reflections (diffraction vectors) in the ZOLZ ($\boldsymbol{g} = \boldsymbol{g_t}$), whereas (8) applies for reflections in HOLZ ($\boldsymbol{g} = \boldsymbol{g_t} + \boldsymbol{g_n}$). $\boldsymbol{g_t}$ and $\boldsymbol{g_n}$ are the components of this HOLZ reflection $\boldsymbol{g}$ at the ZOLZ and perpendicular to it, at the HOLZ the reflection belongs to, respectively.

4. Calculations

4.1. Results from calculations of $\boldsymbol{K_o(\beta)}$ and s_g

The RED method was utilized to elucidate the structural characteristics of a skutterudite CoP_3, which exhibits remarkable thermoelectric properties. In this case, calculations will be presented for one of the series of beam tilting experiments performed for CoP_3 [19]. The various electron diffraction patterns were obtained in SAD mode. Typical patterns of this experiment are presented in Fig. 3, for β = 0.60° (−0.50°), 1.10° (0°) and 1.75° (0.65°) beam tilting angles and for the same goniometer angle. Among them, the pattern in Fig. 3(b) corresponds to the [$\bar{3}$ $\bar{1}$ $\bar{7}$] zone axis of CoP_3. Angles values in parentheses are equal to the difference between the angle of each pattern and [$\bar{3}$ $\bar{1}$ $\bar{7}$] [Fig. 3(b)], whereas numbers outside denote net experimental angles. The coexistence of ZOLZ, as well as second order Laue zone (SOLZ) reflections in all patterns is apparent; furthermore, the presence of SOLZ reflections is quite beneficial for our calculations, as shown in the following sections. It is noteworthy that, as the first order Laue zone (FOLZ) is extinct [29] for the [$\bar{3}$ $\bar{1}$ $\bar{7}$] zone axis, all calculations have been performed for the SOLZ instead.

In order to more efficiently describe the diffraction geometry at the RED tilting experiment of the CoP_3 crystal, the [001] and the [$\bar{3}$ $\bar{1}$ $\bar{7}$] directions of the two zone axes were selected, solely for calculation purposes (i.e. *not experimentally*), to be parallel to the initial incident beam directions. 'Theoretical' analysis by simulations in JEMS was performed using these zone axes as the reference plane, too. Among these two, the [$\bar{3}$ $\bar{1}$ $\bar{7}$] zone axis was selected since an experimental pattern was also encountered in this orientation, Fig. 3(b). The [0 0 1] zone axis was chosen as a common experimental one, yet more simplified case for calculations. Consequently, beta angles values recorded in all tables and results thereafter refer to the relative difference between each tilting angle and the one of the zone axis. The experimental rotation axes for the two cases, [0 0 1] and [$\bar{3}$ $\bar{1}$ $\bar{7}$], will be considered roughly along the [$\bar{1}$ $\bar{1}$ 0] and [1 $\bar{3}$ 0] crystallographic directions respectively; refinement of such axes has been already described [19]. The resulting experimental $\boldsymbol{T}$ vectors are, subsequently, roughly equal to [$\bar{1}$ 1 0] and [$\bar{2}\bar{1}$ $\bar{7}$ 10] ~ [$\bar{2}$ $\bar{1}$ 1], respectively, as derived by Eq. (3).

The results from the calculations of the incident electron beam direction $\boldsymbol{K_o(\beta)}$ as a function of the experimental β angle, using Eq. (2) are illustrated in Table 1. The change in the electron beam directions are clearly illustrated for both cases, [0 0 1] and [$\bar{3}$ $\bar{1}$ $\bar{7}$].

Calculations for the excitation errors ($s_g^{\mathrm{calc.}}$) using both ZOLZ and HOLZ reflections have been accordingly performed and their results are summarized in Table 2.

The 'theoretical' values (s_g^{JEMS}) were obtained by simulations of the SAD patterns in the JEMS software [28]. The derived s_g values from both approaches are in very good agreement, as the errors are only among the 1–2% range; this firmly proves the accuracy of our calculations. A typical example of s_g calculation applying Eqs. (7) and (8) is shown in Appendix B. It has to be noted that the calculated errors for s_g

Table 2
Excitation errors values for the [0 0 1] and [$\bar{3}$ $\bar{1}$ $\bar{7}$] zone axes in RED tilting experiments. The tilting angles used in each zone axis is β = 4.25° for [0 0 1] and β = 0.75° for [$\bar{3}$ $\bar{1}$ $\bar{7}$], respectively.

[uvw] = [0 0 1] β = 4.25°				[uvw] = [$\bar{3}$ $\bar{1}$ $\bar{7}$] β = 0.75°			
Reflections		s_g^{JEMS} (nm^{-1})	$s_g^{\mathrm{calc.}}$ (nm^{-1})	Reflections		s_g^{JEMS} (nm^{-1})	$s_g^{\mathrm{calc.}}$ (nm^{-1})
ZOLZ	FOLZ			ZOLZ	SOLZ		
0 2 0		0.127	0.128	1 $\bar{3}$ 0		−0.021	−0.024
$\bar{1}$ 7 0		0.437	0.439	$\bar{6}$ $\bar{3}$ 3		0.010	0.010
$\bar{15}$ $\bar{1}$ 0		0.471	0.475	$\bar{10}$ $\bar{5}$ 5		−0.111	−0.110
6 10 0		−0.017	−0.015		8 2 $\bar{4}$	0.004	0.002
	10 1 1	0.473	0.466		0 9 1	0.022	0.021
	17 8 1	−0.063	−0.067		$\bar{1}$ $\bar{6}$ 1	0.310	0.305
	18 5 1	−0.327	−0.331		$\bar{3}$ $\bar{14}$ 3	0.021	0.009
	15 $\bar{14}$ 1	−0.464	−0.469		$\bar{2}$ 4 0	0.305	0.309

for reflections nearly in Bragg conditions are somehow higher than 2%. As s_g is significantly small for reflections almost in Bragg, the higher errors in their calculated values may well be attributed to the existence of the smaller, additional components of s_g in the ZOLZ plane (xy plane), along with the main z-component that was considered in the calculations. Close to Bragg conditions, such s_g components at xy plane may be of significance for those small values of the z-component.

4.2. Refinement process of **T** and $\boldsymbol{K_o(0)}$ vectors, [$\bar{3}$ $\bar{1}$ $\bar{7}$] CoP_3 case study

Having configured the geometry in the RED method by defining the rotation axis ***Y***, incident beam direction $\boldsymbol{K_o(\beta)}$, beam tilt path ***T*** and calculating the excitation errors s_g, it is subsequently essential to refine their values [26] as the next step in our calculations.

The refinement of the rotation axis has been already accomplished and results have been published in a previous work [19]. Following this, the beam tilt path will be refined, compared to the more 'coarse' values derived by Eq. (3). For this purpose, HOLZ reflections and their corresponding simulated Kikuchi lines [29,30] will be utilized. This concept was already adopted for PED [24], as Kikuchi lines are very sensitive to tilting experiments and capable of defining Bragg conditions of their corresponding reflections with high accuracy, especially when it comes to HOLZ reflections positioned at a large angle in relation to the rotation axis.

In more detail, during the RED tilting experiment in our case study, the low symmetry -i.e. with a large number of independent reflections- [$\bar{3}$ $\bar{1}$ $\bar{7}$] pattern, was selected as the reference plane, Fig. 4. In this pattern, HOLZ reflections would be positioned in between the ZOLZ ones, which makes refinement process handier, too.

The refinement methodology assumes that, coincidentally, for a given tilting angle β during a beam or goniometer tilt experiment, two or more HOLZ reflections would be found to satisfy Bragg conditions. Such reflections have been chosen in the reference plane [$\bar{3}$ $\bar{1}$ $\bar{7}$] of Fig. 4 for two tilting angles in relation to the [$\bar{3}$ $\bar{1}$ $\bar{7}$] β angle, $\beta_i = 0.75^\circ$ ($\boldsymbol{g_1}$ = 8 2 $\bar{4}$ and $\boldsymbol{g_2}$ = 7 5 $\bar{4}$) and $\beta_j = -0.70^\circ$ ($\boldsymbol{g_3}$ = $\bar{2}$ $\bar{10}$ 2 and $\boldsymbol{g_4}$ = $\bar{8}$ 8 2). Beyond experimental evidence, Bragg conditions were additionally confirmed by simulated SAD patterns by JEMS. The projected position of the simulated Kikuchi deficiency lines in the exact zone axis orientation of such a HOLZ reflection was determined by simple reciprocal vector analysis, as shown for instance for the $\boldsymbol{g_1}$ = 8 2 $\bar{4}$ and $\boldsymbol{g_2}$ = 7 5 $\bar{4}$ reflections and their corresponding Kikuchi lines, K_{i1} and K_{i2} (blue coloured) or the $\boldsymbol{g_3}$ = $\bar{2}$ $\bar{10}$ 2 and $\boldsymbol{g_4}$ = $\bar{8}$ 8 2 and K_{j1} and K_{j2} ones (green coloured). The points of coincidence of each pair of simulated Kikuchi lines ($K_{i1} - K_{i2}$ and $K_{j1} - K_{j2}$) define individual $\boldsymbol{T_{\beta i}}$ and $\boldsymbol{T_{\beta j}}$ sub-vectors, as shown in Fig. 4. These sub-vectors can be calculated and determined using basic vector analysis, too. Calculations are still performed using this ZOLZ reference plane, as in previous sections and analysis follows an analogous line of reasoning, as presented in Appendices A and B. In this way, several $\boldsymbol{T_\beta}$ sub-vectors are calculated and, eventually, the beam tilt path $\boldsymbol{T_i}$ is determined by the vectorial difference of any two $\boldsymbol{T_\beta}$, as shown in Eq. (9) and also illustrated in Fig. 4:

$$\boldsymbol{T_i} = \boldsymbol{T_{\beta i}} - \boldsymbol{T_{\beta j}} \tag{9}$$

Using this way of thinking, several $\boldsymbol{T_i}$ vectors were calculated and the results are summarised in Table 3.

The results of the $\boldsymbol{T_i}$ vector refinement reveal that the determined values are quite close to each other and in good agreement with the 'coarser' one ([$\overline{21}$ $\bar{7}$ 10] ~ [$\bar{2}$ $\bar{1}$ 1]). In order to further increase accuracy, statistical analysis was performed at the various $\boldsymbol{T_i}$ values and their mean value was calculated:

$$\boldsymbol{T_{mean}} = [\overline{20.5}\ \overline{8.1}\ 10.0] = [\overline{2.05}\ \overline{0.81}\ 1.00].$$

The angular difference between the two vectors, T = [$\overline{21}$ $\bar{7}$ 10] and $\boldsymbol{T_{mean}}$ = [$\overline{20.5}$ $\overline{8.1}$ 10] is $\varphi_T = 2.85^\circ$, which furthermore establishes the necessity for a refinement process. In addition, a solid proof for refinement accomplishment was the low value of the standard error σ_T, which was among the 4–10% range for every one of the three $\boldsymbol{T_i}$ components. The calculation accuracy of $\boldsymbol{T_i}$ is directly proportional to the amount of experimental results that can be obtained and included in the statistical analysis. Refinement is, therefore, heavily dependent on the frequency that HOLZ reflections appear in Bragg during a RED beam or goniometer tilting experiment. This also adds to the need to perform RED experiments with large goniometer tilting angles and fine tilt steps [4], the latter using the beam tilt option.

Increased accuracy in structure determination in RED also requires the refinement of the initial electron beam direction $\boldsymbol{K_o(0)}$, i.e. the one which was chosen to be parallel to the zone axis used as the reference point in the RED method analysis. In order to accomplish this, ZOLZ and/or HOLZ reflections that satisfy Bragg conditions for any given experimental tilting angle β are utilised during a RED tilting experiment. In Bragg conditions, the excitation error for such a reflection is zero, therefore Eq. (6) becomes:

$$-2\boldsymbol{K_o}(\beta)\cdot\boldsymbol{g} - \boldsymbol{g}^2 = 0 \tag{10}$$

By finding reciprocal vectors $\boldsymbol{g}$ in Bragg, the direction of $\boldsymbol{K_o(\beta)}$ can be determined for any experimental angle β. At least three $\boldsymbol{g}$ vectors are necessary, in order all the three components ($\boldsymbol{K_o(\beta)_x}$, $\boldsymbol{K_o(\beta)_y}$, $\boldsymbol{K_o(\beta)_z}$) of the $\boldsymbol{K_o(\beta)}$ vector to be calculated. The results from the calculations are summarised in Table 4.

Following this, the (β, $\boldsymbol{K_o(\beta)}$) pairs can be substituted in Eq. (2), which takes the equivalent form:

$$\boldsymbol{K_o}(\beta) = \boldsymbol{K_o}(0) + (n\ \boldsymbol{T})\beta \tag{11}$$

This clearly shows the linear relationship between β and $\boldsymbol{K_o(\beta)}$, in the well know form of $f(X) = \boldsymbol{a} + \boldsymbol{b}\ X$, therefore linear regression analysis and the least squares method can be exploited for statistical analysis of the calculations. This linear relationship for each of the three components of the $\boldsymbol{K_o(\beta)}$ vector, $\boldsymbol{K_o(\beta)_x}$, $\boldsymbol{K_o(\beta)_y}$, $\boldsymbol{K_o(\beta)_z}$ is best denoted below:

$$\boldsymbol{K_o}(\beta)_x = \boldsymbol{K_o}(0)_x + (n\ \boldsymbol{T}_x)\beta \tag{12}$$

$$\boldsymbol{K_o}(\beta)_y = \boldsymbol{K_o}(0)_y + (\mathrm{n}\ \boldsymbol{T}_y)\beta \tag{13}$$

$$\boldsymbol{K_o}(\beta)_z = \boldsymbol{K_o}(0)_z + (\mathrm{n}\ \boldsymbol{T}_z)\beta \tag{14}$$

Their common plot is shown in more detail in Fig. 5.

The incident beam direction $\boldsymbol{K_o(0)}$ is then derived by the y-intercept of the least squares line and is given by the formula:

$$\boldsymbol{K_o}(0) = [\Sigma_i \boldsymbol{K_o}(\beta) - n\boldsymbol{T}(\Sigma_i\beta)]/\mathrm{N} \tag{15}$$

In addition, the slope of the same line enables to determine the beam tilt path ***T***, as follows:

$$n\boldsymbol{T} = [\mathrm{N}\Sigma_i(\beta\boldsymbol{K_o}(\beta)) - \Sigma_i\beta\Sigma_i\boldsymbol{K_o}(\beta)]/[N\Sigma_i\beta^2 - (\Sigma_i\beta)^2] \tag{16}$$

Calculations for the determination of the $\boldsymbol{K_o(0)}$ using this approach have been performed for the case of the [$\bar{3}$ $\bar{1}$ $\bar{7}$] zone axis [Fig. 3(b)], as this was experimentally encountered. Applying the least squares refinement, the normalized value of $\boldsymbol{K_o(0)}$ was found to be

$$\boldsymbol{K_o}(0) = [3.03\ 1.00\ 7.07]$$

which is very close to the opposite of the [$\bar{3}$ $\bar{1}$ $\bar{7}$] zone axis. In fact, the two $\boldsymbol{K_o(0)}$ vectors, [3 1 7] ('nominal') and [3.03 1.00 7.07] (refined) have an angular difference of only $\varphi_{\boldsymbol{K_o}(0)} = 0.07^\circ$ revealing that the methodology in this study bears high accuracy. Furthermore, the beam tilt path was determined to be equal to

$$\boldsymbol{T} = [\overline{2.21}\ \overline{0.77}\ 1.00]$$

which is also a quite satisfactory result (angular difference is only $\varphi'_T = 1.37^\circ$ in this case), in very good agreement with its refined value calculated above.

The calculated and refined values of all vectors necessary to clarify the RED experiment diffraction geometry (***Y***, $\boldsymbol{K_o(\beta)}$, $\boldsymbol{K_o(0)}$, ***T***) can be merely used as an input for the excitation errors calculations using Eqs.

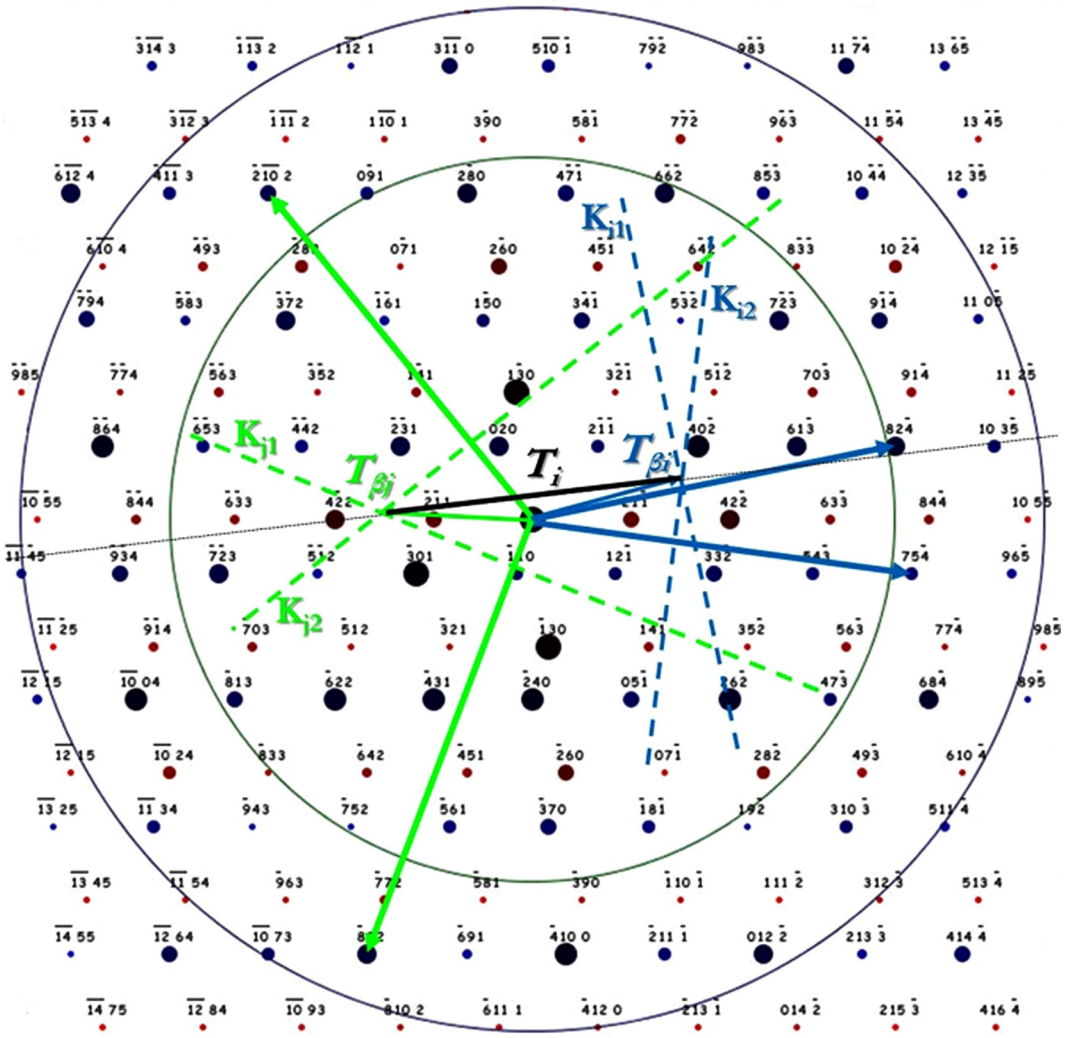

Fig. 4. Beam tilt path refinement process using simulated Kikuchi lines of HOLZ reflections in [$\bar{3}$ $\bar{1}$ $\bar{7}$] zone axis pattern of CoP_3. Red and blue spots denote ZOLZ and SOLZ reflections, respectively. Dark red or blue spots illustrate the strongest reflections of both orders. (For interpretation of the references to colour in this figure legend, the reader is referred to the web version of this article.)

(7) or (8), for both the [0 0 1] and [$\bar{3}$ $\bar{1}$ $\bar{7}$] zone axes. It is obvious that, by incorporating the vectors' refined values in these equations, the accuracy in s_g is further increased and subsequent calculations can be performed in a robust way.

The increased accuracy in s_g will form a solid input for the next step in structure determination using RED, which is the theoretical calculation of diffracted beam structure factors and intensities using the Bloch wave methodology. Refined values of s_g of such reflections might be used in a many beam dynamical case in RED. In terms of experimental measurements, the refined excitation error values can be used in

Table 3
T vector refinement results. Analysis was performed in the [$\bar{3}$ $\bar{1}$ $\bar{7}$] zone axis during the RED tilting experiment.

#	β (°)	Reflections in Bragg		$T_{\beta i}$	$T_{\beta j}$	T_i
1	−0.70	$\bar{2}$ $\bar{10}$ 2	$\bar{8}$ 8 2	[$\bar{3.02}$ $\bar{1.67}$ 1.54]		**[$\bar{1.}$ **$\bar{97}$** $\bar{1.}$ **$\bar{10}$** 1.00]**
2	−0.15	$\bar{4}$ $\bar{11}$ 3	$\bar{11}$ 3 4		[$\bar{0.60}$ $\bar{0.32}$ 0.30]	
1	−0.70	$\bar{2}$ $\bar{10}$ 2	$\bar{8}$ 8 2	[$\bar{3.02}$ $\bar{1.67}$ 1.54]		**[$\bar{1.}$ **$\bar{96}$** $\bar{0.}$ **$\bar{87}$** 1.00]**
3	−0.15	$\bar{11}$ 3 4	2 13 $\bar{3}$		[$\bar{0.67}$ $\bar{0.66}$ 0.38]	
1	−0.70	$\bar{2}$ $\bar{10}$ 2	$\bar{8}$ 8 2	[$\bar{3.02}$ $\bar{1.67}$ 1.54]		**[$\bar{2.}$ **$\bar{05}$** $\bar{0.}$ **$\bar{85}$** 1.00]**
4	1.35	$\bar{13}$ $\bar{3}$ 6	7 $\bar{2}$ $\bar{3}$		[6.32 2.23 $\bar{3.03}$]	
1	−0.70	$\bar{2}$ $\bar{10}$ 2	$\bar{8}$ 8 2	[$\bar{3.02}$ $\bar{1.67}$ 1.54]		**[$\bar{2.}$ **$\bar{13}$** $\bar{0.}$ **$\bar{61}$** 1.00]**
5	0.75	7 5 $\bar{4}$	8 2 $\bar{4}$		[3.83 0.27 $\bar{1.68}$]	
2	−0.15	$\bar{4}$ $\bar{11}$ 3	$\bar{11}$ 3 4	[$\bar{0.60}$ $\bar{0.32}$ 0.30]		**[$\bar{2.}$ **$\bar{08}$** $\bar{0.}$ **$\bar{76}$** 1.00]**
4	1.35	$\bar{13}$ $\bar{3}$ 6	7 $\bar{2}$ $\bar{3}$		[6.32 2.23 $\bar{3.03}$]	
3	−0.15	$\bar{11}$ 3 4	2 13 $\bar{3}$	[$\bar{0.67}$ $\bar{0.66}$ 0.38]		**[$\bar{2.}$ **$\bar{05}$** $\bar{0.}$ **$\bar{85}$** 1.00]**
4	1.35	$\bar{13}$ $\bar{3}$ 6	7 $\bar{2}$ $\bar{3}$		[6.32 2.23 $\bar{3.03}$]	
3	−0.15	$\bar{11}$ 3 4	2 13 $\bar{3}$	[$\bar{0.67}$ $\bar{0.66}$ 0.38]		**[$\bar{2.}$ **$\bar{18}$** $\bar{0.}$ **$\bar{46}$** 1.00]**
5	0.75	7 5 $\bar{4}$	8 2 $\bar{4}$		[3.83 0.27 $\bar{1.68}$]	

Table 4
Results from the calculations of $K_o(\beta)$ as a function of beta angle during the RED beam tilting experiment. The [$\bar{3}$ $\bar{1}$ $\bar{7}$] zone axis is again used as a reference.

#	β (°)	Reflections in Bragg					$K_o(\beta)$
		ZOLZ		SOLZ			
1	−0.70	6 3 $\bar{3}$		$\bar{2}$ $\bar{10}$ 2	$\bar{8}$ 8 2		**[3.07 1.00 7.38]**
2	−0.15			$\bar{4}$ $\bar{11}$ 3	$\bar{11}$ 3 4	12 $\bar{3}$ $\bar{5}$	**[3.01 1.00 7.08]**
3	−0.15			12 $\bar{3}$ $\bar{5}$	$\bar{4}$ $\bar{11}$ 3	$\bar{7}$ $\bar{9}$ 4	**[3.05 1.00 7.15]**
4	−0.15			$\bar{4}$ $\bar{11}$ 3	$\bar{7}$ $\bar{9}$ 4	$\bar{11}$ 3 4	**[3.00 1.00 7.00]**
5	−0.15			2 13 $\bar{3}$	12 $\bar{3}$ $\bar{5}$	$\bar{4}$ $\bar{11}$ 3	**[3.03 1.00 7.11]**
6	0.75			7 5 $\bar{4}$	8 2 $\bar{4}$	$\bar{11}$ $\bar{11}$ 6	**[3.06 1.00 6.87]**
7	0.75	$\bar{7}$ 0 3		7 5 $\bar{4}$	8 2 $\bar{4}$		**[3.06 1.00 6.90]**
8	0.75			$\bar{11}$ $\bar{11}$ 6	$\bar{9}$ 11 2	7 5 $\bar{4}$	**[2.99 1.00 6.76]**
9	1.35	$\bar{13}$ $\bar{3}$ 6		7 $\bar{2}$ $\bar{3}$	$\bar{7}$ $\bar{16}$ 5		**[3.03 1.00 6.67]**
10	1.35			4 7 $\bar{3}$	7 $\bar{2}$ $\bar{3}$	$\bar{7}$ $\bar{16}$ 5	**[3.02 1.00 6.64]**
11	1.35	$\bar{4}$ 5 1	$\bar{9}$ $\bar{8}$ 5	7 $\bar{2}$ $\bar{3}$			**[3.01 1.00 6.63]**
12	1.35			7 $\bar{2}$ $\bar{3}$	5 $\bar{10}$ $\bar{1}$	4 7 $\bar{3}$	**[3.02 1.00 6.63]**

the measurements of integrated intensities of diffracted beams, which would be equal to the area under their rocking curves, i.e. when measured intensities are plotted against s_g. Having efficaciously refined s_g, by the methodology presented in this study, results from the two complementary approaches –theoretical and experimental- may be compared, so that structure parameters can be subsequently elucidated. This is important for a wide range of technology-based materials in general and, in particular, for CoP_3 thermoelectrics, because of their property monitoring due to thermal parameter (Debye-Waller factors) precise calculations. This provides the initiative for a continuation of the current work and can be well attempted in a future study.

5. Conclusions

In this work, a universal methodology to carry out precise diffraction conditions as a function of the experimental beam or goniometer tilting angle β during data collection in the Rotation Electron Diffraction technique has been described, based on the acquisition of a series of experimental diffraction patterns. The approach involved determination and calculation of the incident electron beam direction $K_o(\beta)$ as a function of angle β and its beam tilt path T during RED. The RED method geometry determination has been applied to thermoelectric materials and a CoP_3 crystal was selected for that purpose. A refinement procedure for $K_o(\beta)$ or $K_o(0)$ and T has been subsequently described, in order to further increase experimental data accuracy. These quantities formed the perquisites for calculation of excitation errors for ZOLZ and/or HOLZ reflections and their corresponding formulas have been successfully derived and refined, too. The excitation errors values, calculated based on refined $K_o(0)$ and T, can be included in both the experimental integrated intensities measurements and also in the theoretical ones, derived using the Bloch wave method and subsequently compared. In this way, the most important structural parameters can be satisfactorily refined, paving the way to enhanced accuracy in structure determination. It has been demonstrated that diffraction geometry calculations and refinement in RED are quite essential as they enable incorporation of dynamical contributions among electron beams in a concrete and precise manner and, in principle, can result in higher accuracy structural parameter results. The latter is especially important in the case for thermal parameters -i.e. Debye-Waller factors- determination in thermoelectric materials, which are critical factors for their properties' evaluation and subsequent improvement.

Acknowledgements

Contributions to this work by Mika Buxhuku (CoP_3 synthesis and RED experimental acquisition (Fig. 3)), Ole Bjørn Karlsen (CoP_3 synthesis), Alexandra Evangelou (assistance with T_β sub-vector calculation) and Peter Oleynikov (RED set up, acquisition (Fig. 3) and analysis at the University of Stockholm) are gratefully acknowledged.

Funding sources

This work received funding by the University of Stavanger, Norway (grant number 8500).

Author contributions

V.H. and J.G. designed the calculation approach. A.D. and V.H. refined and conducted the calculations and derived the final formulas. A.D. was involved in the interpretation of results, developed the programming codes and performed simulations of the calculated data. V.H. also contributed to experimental results acquisition.

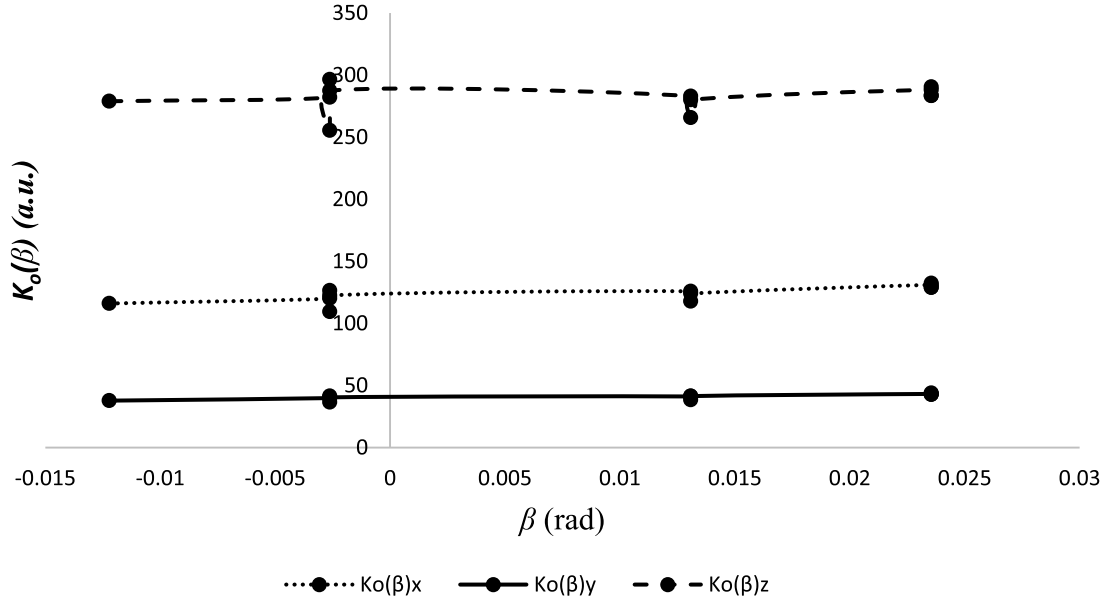

Fig. 5. Plot of the three $K_o(\beta)_x$, $K_o(\beta)_y$, $K_o(\beta)_z$ components as a function of experimental tilting angle β. A linear relationship is illustrated. Results are shown in non-normalized values.

All authors have approved the final, submitted version of the article.

Declarations of interest

None.

Appendix A. Analysis of g vectors in their components along u_1, u_2 and u_3 unit vectors

Using Eq. (1), any diffraction vector can be analysed in three components along $\boldsymbol{u_1}$, $\boldsymbol{u_2}$ and $\boldsymbol{u_3}$. This includes either ZOLZ or HOLZ vectors and facilitates calculations of excitation errors and all other quantities of RED geometry.

As an example, the [0 0 1] zone axis of CoP_3 (lattice constant $a = 0.77$ nm) is used. The three unit vectors are $\boldsymbol{u_1} = [0\ 0\ 1]$, $\boldsymbol{u_2} = [\bar{1}\ \bar{1}\ 0]$, $\boldsymbol{u_3} = [1\ \bar{1}\ 0]$ and a FOLZ diffraction vector $\boldsymbol{g_1} = [9\ \bar{6}\ 1]$ will be analysed as follows:

$\boldsymbol{g}_1 = [9\,\bar{6}\,1] = g_{11}[0\ 0\ 1] + g_{12}[\bar{1}\ \bar{1}\ 0] + g_{13}[1\ \bar{1}\ 0]$.

This results in a system of three equations with three unknown values, g_{11}, g_{12} and g_{13}, as follows (g_{11}, g_{12} and g_{13} are either integer or decimal numbers):

$0g_{11} - 1g_{12} + 1g_{13} = 9$

$0g_{11} - 1g_{12} - 1g_{13} = -6$

$1g_{11} + 0g_{12} + 0g_{13} = 1$

whose solution is $g_{11} = 1$, $g_{12} = -1.5$ and $g_{13} = 7.5$. Consequently, the vector $\boldsymbol{g_1} = [9\ \bar{6}\ 1]$ is rewritten as:

$\boldsymbol{g}_1 = [9\ \bar{6}\ 1] = 1[0\ 0\ 1] - 1.5[\bar{1}\ \bar{1}\ 0] + 7.5[1\ \bar{1}\ 0]$.

Appendix B. Excitation errors calculations for ZOLZ or HOLZ reflections

A characteristic example of the excitation error calculations for the $\boldsymbol{g_1} = [9\ \bar{6}\ 1]$ FOLZ reflection is given for the [0 0 1] zone axis of CoP_3 ($a = 0.77$ nm) and a beam tilting angle of $\beta = 4.25^\circ = 0.0743$ rad. The analysis of the $\boldsymbol{g_1}$ vector has been already performed in Appendix A, in addition, the $\boldsymbol{T}$ vector, as derived by Eq. (3) is

$T = [\bar{1}\ \bar{1}\ 0] \times [0\ 0\ 1] = [\bar{1}\ 1\ 0]$.

Defining the value of the $\boldsymbol{K_o(\beta)}$ vector for the specific angle β, using Eq. (2) is the first step towards s_g calculation. In more detail:

$$\boldsymbol{K_o}(\beta) = \boldsymbol{K_o}(0) + n\,\beta T \tag{B.1}$$

or,

$$\boldsymbol{K_o}(\beta) = k\,\boldsymbol{K_o}(0) + \beta(k/|\boldsymbol{T}|)\boldsymbol{T} \tag{B.2}$$

where $k = 1/\lambda = 398.4064\ \mathrm{nm}^{-1}$, for 200 keV electrons and $|\boldsymbol{T}| = 1.8366\ \mathrm{nm}^{-1}$ is the magnitude of the $\boldsymbol{T}$ vector. By substituting all values in Eq. (B.2), the value of $\boldsymbol{K_o(\beta)}$ is equal to

$\boldsymbol{K_o}(\beta) = [\overline{16.12}\ 16.12\ \overline{398.41}] = [\overline{0.04}\ 0.04\ \bar{1}]$.

As $\boldsymbol{g_1} = [9\ \bar{6}\ 1]$ is a HOLZ reflection, Eq. (8) will be used in order to estimate the excitation error. The $\boldsymbol{T}$ vector needs also be analysed into its components along the three $\boldsymbol{u_1} = [0\ 0\ 1]$, $\boldsymbol{u_2} = [\bar{1}\ \bar{1}\ 0]$ and $\boldsymbol{u_3} = [1\ \bar{1}\ 0]$ unit vectors, so analysis is facilitated, as follows (see Appendix A):

$\boldsymbol{T} = [\bar{1}\ 1\ 0] = T_{11}[0\ 0\ 1] + T_{12}[\bar{1}\ \bar{1}\ 0] + T_3[1\ \bar{1}\ 0]$, or

$\boldsymbol{T} = [\bar{1}\ 1\ 0] = 0\ [0\ 0\ 1] + 0\ [\bar{1}\ \bar{1}\ 0] - 1\ [1\ \bar{1}\ 0]$.

Following this, the $s_{g1}^{calc.}$ calculation is:

$$2ks_{g1}^{calc.} = -2n\beta\boldsymbol{T}\cdot\boldsymbol{g_{t1}} - 2\boldsymbol{K_o}(0)\cdot\boldsymbol{g_{n1}} - \boldsymbol{g}_1^2 \tag{B.3}$$

$$s_{g1}^{calc.} = (k/|\boldsymbol{K_o}(\beta)||\boldsymbol{T}|)\beta\boldsymbol{T}\cdot\boldsymbol{g_{t1}} - (k/|\boldsymbol{K_o}(\beta)|)|\boldsymbol{g_{n1}}| - (1/2k)\boldsymbol{g}_1^2 \tag{B.4}$$

In Eq. (B.4), $|\boldsymbol{K_o(\beta)}| = 399.058\ \mathrm{nm}^{-1}$ and $|\boldsymbol{g_{n1}}| = 1.2987\ \mathrm{nm}^{-1}$ are the magnitudes of the $\boldsymbol{K_o(\beta)}$ and the $\boldsymbol{g_{n1}}$ vectors, respectively. After the calculations, the value of $s_{g1}^{calc.}$ for the $\boldsymbol{g_1} = [9\ \bar{6}\ 1]$ reflection is

$s_{g1}^{calc.} = 0.0234\ \mathrm{nm}^{-1}$.

Supplementary material

Supplementary material associated with this article can be found, in the online version, at doi:10.1016/j.ultramic.2019.02.011.

References

[1] R. Vincent, P.A. Midgley, Double conical beam-rocking system for measurement of integrated electron diffraction intensities, Ultramicroscopy 53 (3) (1994) 271–282 https://doi.org/10.1016/0304-3991(94)90039-6.

[2] U. Kolb, T. Gorelik, C. Kübel, M.T. Otten, D. Hubert, Towards automated diffraction tomography: part i—data acquisition, Ultramicroscopy 107 (6–7) (2007) 507–513 https://doi.org/10.1016/j.ultramic.2006.10.007.

[3] E. Mugnaioli, T. Gorelik, U. Kolb, "Ab initio" structure solution from electron diffraction data obtained by a combination of automated diffraction tomography and precession technique, Ultramicroscopy 109 (2009) 758–765 https://doi.org/10.

1016/j.ultramic.2009.01.011.
[4] D. Zhang, P. Oleynikov, S. Hovmöller, X. Zou, Collecting 3D electron diffraction data by the rotation method, Z. Kristallogr 225 (2010) 94–102 https://doi.org/10.1524/zkri.2010.1202.
[5] W. Wan, J. Sun, J. Su, S. Hovmöller, X.D. Zou, Three-dimensional rotation electron diffraction: software RED for automated data collection and data processing, J. Appl. Cryst. 46 (2013) 1863–1873 https://doi.org/10.1107/S0021889813027714.
[6] A. Mayence, J.R.G. Navarro, Y. Ma, O. Terasaki, L. Bergström, P. Oleynikov, Phase identification and structure solution by three-dimensional electron diffraction tomography: Gd − phosphate nanorods, Inorg. Chem. 53 (2014) 5067–5072 https://doi.org/10.1021/ic500056r.
[7] Z. Dauter, Data collection strategies, Acta Cryst. D 55 (1999) 1703–1717 https://doi.org/10.1107/S0907444999008367.
[8] J. Su, E. Kapaca, L. Liu, V. Georgieva, W. Wan, J. Sun, V. Valtchev, S. Hovmöller, X. Zou, Structure analysis of zeolites by rotation electron diffraction (RED), Microporous Mesoporous Mater. 189 (2014) 115–125 https://doi.org/10.1016/j.micromeso.2013.10.014.
[9] T. Willhammar, Y. Yun, X. Zou, Structural determination of ordered porous solids by electron crystallography, Adv. Funct. Mater. 24 (2014) 182–199 https://doi.org/10.1002/adfm.201301949.
[10] K. Zhang, H. Chen, X. Wang, D. Guo, C. Hu, J. Sun, S. Wang, Q. Leng, Synthesis and structure determination of potassium copper selenide nanowires and solid-state supercapacitor application, J. Power Sources 268 (2014) 522–532 https://doi.org/10.1016/j.jpowsour.2014.06.079.
[11] B. Wang, T. Rhauderwiek, A.K. Inge, H. Xu, T. Yang, Z. Huang, N. Stock, X. Zou, A porous cobalt tetraphosphonate metal–organic framework: accurate structure and guest molecule location determined by continuous-rotation electron diffraction, Chem. Eur. J. 24 (2018) 17429–17433 https://doi.org/10.1002/chem.201804133.
[12] Y. Yun, W. Wan, F. Rabbani, J. Su, H. Xu, S. Hovmöller, M. Johnsson, X. Zou, Phase identification and structure determination from multiphase crystalline powder samples by rotation electron diffraction, J. Appl. Cryst. 47 (2014) 2048–2054 https://doi.org/10.1107/S1600576714023875.
[13] D. Singh, Y. Yun, W. Wan, B. Grushko, X. Zou, S. Hovmöller, Structure determination of a pseudo-decagonal quasicrystal approximant by the strong-reflections approach and rotation electron diffraction, J. Appl. Cryst. 49 (2016) 433–441 https://doi.org/10.1107/S1600576716000042.
[14] Y. Wang, S. Takki, O. Cheung, H. Xu, W. Wan, L. Öhrström, A.K. Inge, Elucidation of the elusive structure and formula of the active pharmaceutical ingredient bismuth subgallate by continuous rotation electron diffraction, Chem. Comm. 53 (2017) 7018–7021, https://doi.org/10.1039/c7cc03180g https://doi.org/.
[15] Y. Wang, T. Yang, H. Xu, X. Zou, W. Wan, On the quality of the continuous rotation electron diffraction data for accurate atomic structure determination of inorganic compounds, J. Appl. Cryst. 51 (2018) 1094–1101 https://doi.org/10.1107/S1600576718007604.
[16] M.O. Cichocka, J. Ångström, B. Wang, X. Zou, S. Smeets, High-throughput continuous rotation electron diffraction data acquisition *via* software automation, J. Appl. Cryst 51 (2018) 1652–1661 https://doi.org/10.1107/S1600576718015145.
[17] E. van Genderen, M.T.B. Clabbers, P.P. Das, A. Stewart, I. Nederlof, K.C. Barentsen, Q. Portillo, N.S. Pannu, S. Nicolopoulos, T. Gruene, J.P. Abrahams, Ab initio structure determination of nanocrystals of organic pharmaceutical compounds by electron diffraction at room temperature using a Timepix quantum area direct electron detector, Acta Cryst. A 72 (2016) 236–242 http://dx.doi.org/10.1107/S2053273315022500.
[18] M. Buxhuku, V. Hansen, J. Gjønnes, The measurement of intensities in the rotation electron diffraction technique, Micron 101 (2017) 103–107 https://dx.doi.org/10.1016/j.micron.2017.06.006.
[19] M. Buxhuku, V. Hansen, P. Oleynikov, J. Gjønnes, The determination of rotation axis in the rotation electron diffraction technique, Microsc. Microanal. 19 (2013) 1276–1280 https://doi.org/10.1017/S1431927613012749.
[20] G.S. Polymeris, N. Vlachos, A.U. Khan, E. Hatzikraniotis, Ch.B. Lioutas, A. Delimitis, E. Pavlidou, K.M. Paraskevopoulos, Th. Kyratsi, Nanostructure and doping stimulated phase separation in high-*ZT* $Mg_2Si_{0.55}Sn_{0.4}Ge_{0.05}$ compounds, Acta Mater 83 (2015) 285–293 https://dx.doi.org/10.1016/j.actamat.2014.09.031.
[21] W. Sinkler, L.D. Marks, Characteristics of precession electron diffraction intensities from dynamical simulations, Z. Kristallogr 225 (2010) 47–55 https://doi.org/10.1524/zkri.2010.1199.
[22] L. Palatinus, D. Jacob, P. Cuvillier, M. Klementová, W. Sinkler, L.D. Marks, Structure refinement from precession electron diffraction data, Acta Cryst. A 69 (2013) 171–188 https://doi:10.1107/S010876731204946X.
[23] K. Gjønnes, Y. Cheng, B.S. Berg, V. Hansen, Corrections for multiple scattering in integrated electron diffraction intensities. Application to determination of structure factors in the [001]Projection of Al_mFe, Acta Cryst. A 54 (1998) 102–119 https://doi.org/10.1107/S0108767397009963.
[24] K. Gjønnes, On the integration of electron diffraction intensities in the Vincent-Midgley precession technique, Ultramicroscopy 69 (1997) 1–11 https://doi.org/10.1016/S0304-3991(97)00031-4.
[25] P. Oleynikov, S. Hovmöller, X.D. Zou, Precession electron diffraction: observed and calculated intensities, Ultramicroscopy 107 (2007) 523–533 https://doi.org/10.1016/j.ultramic.2006.04.032.
[26] L. Palatinus, V. Petříček, C.A. Corrêa, Structure refinement using precession electron diffraction tomography and dynamical diffraction: theory and implementation, Acta Cryst. A 71 (2) (2015) 235–244 https://doi.org/10.1107/S2053273315001266.
[27] S. Diplas, Ø. Prytz, O.B. Karlsen, J.F. Watts, J. Taftø, A quantitative study of valence electron transfer in the skutterudite compound CoP_3 by combining x-ray induced Auger and photoelectron spectroscopy, J. Phys.: Condens. Matter 19 (2007) 246216https://doi:10.1088/0953-8984/19/24/246216.
[28] P. Stadelmann, JEMS Manual, http://www.jems-saas.ch/.
[29] J.C.H. Spence, J.M. ZuO, Electron Microdiffraction, Plenum Press, New York, 1992, pp. 20–28.
[30] D.B. Williams, C.B. Carter, Transmission Electron Microscopy – A Textbook for Materials Science, second edition, Springer, New York, 2009, pp. 311–322.